Received 26 January 2024; revised 15 April 2024; accepted 31 May 2024.
Date of publication 12 June 2024; date of current version 20 June 2024.

Digital Object Identifier 10.1109/OAJPE.2024.3413606

Estimating Aggregate Capacity of Connected DERs and Forecasting Feeder Power Flow With Limited Data Availability

AMIR REZA NIKZAD[1], AMR ADEL MOHAMED[1] (Senior Member, IEEE), BALA VENKATESH[1] (Senior Member, IEEE), AND JOHN PENARANDA[2]

[1]Department of Electrical, Computer and Biomedical Engineering, Toronto Metropolitan University, Toronto, ON M5B 2K3, Canada
[2]Hydro One, Toronto, ON M5G 1P5, Canada

CORRESPONDING AUTHOR: B. VENKATESH (bala@torontomu.ca)

This work was supported in part by the Natural Sciences and Engineering Research Council of Canada (NSERC) and in part by the Mathematics of Information Technology and Complex Systems (MITACS).

ABSTRACT By 2050, zero-carbon electric power systems will rely heavily on innumerable distributed energy resources (DERs), such as wind and solar. Accurate estimation of the aggregate connected DER capacity becomes pivotal in such a landscape. However, forecasting, power flow analysis, and optimization of feeders for operational decision-making by individually modeling each of these numerous renewables in the absence of complete information are operationally challenging and technically impractical. In response, we introduce a method to accurately estimate the aggregate capacities of the connected DERs on distribution feeders and a near-term forecasting method. Our proposal comprises: 1) ovel deep learning-based architecture with a few convolutional neural network and long short-term memory (CNN-LSTM) modules to represent feeder connected aggregate models of DERs and loads and associated training algorithms; 2) method for estimating aggregate capacities of connected renewables and loads; and 3) method for short-term (hourly) high-resolution forecasting. This step of estimation of the aggregate capacities of connected DERs, is a sequel to solving feeder hosting capacity problem. The method is tested using a North American utility feeder data, achieving an average accuracy of 95.56% for forecasting aggregate load power, 93.70% for feeder flow predictions, and 97.53% for estimating the aggregate capacity of DERs.

INDEX TERMS Aggregate connected renewables, deep neural network (DNN), distributed energy resources (DERs), estimation, forecasting.

NOMENCLATURE

Indices

t	Time index of time step (one hour).
i	Scenario index of considered DERs' capacities.

Parameters and Variables

N_{SC}	Total number of scenarios.
$C_{w,i}/C_{s,i}$	Wind / solar aggregate capacity considered for each scenario i.
$P^t_{w,i}$	Aggregate wind power at scenario i and time t.
$P^t_{s,i}$	Aggregate solar power at scenario i and time t.
$P^t_{l,i}$	Aggregate load power calculated at scenario i.
P^t_m	Feeder power reading at time t.
$\hat{\boldsymbol{P}}^t_{\boldsymbol{m}}$	Predicted feeder power at time t.
ρ^t_w/ρ^t_s	Per unit wind / solar power profile at time t.
p_w/p_s	Standard wind / solar power based on weather data.
X_w/X_s	Input features for the wind / solar CNN-LSTM model.
$X^{(1)}_l/X^{(2)}_l$	Input features for the load model #1 / #2.
P^t_L	Load power calculated for training load model #2.
$\hat{\boldsymbol{P}}^t_{\boldsymbol{l_1,i}}$	Predicted aggregate load power derived from the load model #1 for each scenario i.
$\hat{\boldsymbol{P}}^t_{\boldsymbol{L}}$	Predicted aggregate load power derived from the load model #2.
f_w/f_s	CNN-LSTM models for wind / solar power training.

$f_{l_1}^{(i)}$	CNN-LSTM models for load model #1 at scenario i.
f_{l_2}	CNN-LSTM models for load model #2.
$\bar{C}_w/\bar{C}_s$	Estimated aggregate wind / solar capacity for each feeder.

Acronyms

ADMS	Advanced distribution management system.
AI	Artificial intelligence.
ANN	Artificial neural network.
ASPC	Aggregate solar power capacity.
AWPC	Aggregate wind power capacity.
BTM	Behind the meter.
CNN	Convolutional neural network.
DER	Distributed energy resources.
DNN	Deep neural network.
EV	Electric vehicle.
GHG	Greenhouse gas.
LSTM	Long short-term memory.
MSE	Mean squared error
MV	Medium voltage.
NERC	North American electric reliability corporation.
PU	Per unit.
PV	Photovoltaic.
ReLU	Rectified linear unit
RMSE	Root mean square error.
SCADA	Supervisory control and data acquisition.
STLF	Short-term load forecasting.
TOA	Top of atmosphere.

I. INTRODUCTION

ENVIRONMENTAL problems with catastrophic consequences are caused by global warming, which results from the emission of greenhouse gases by burning fossil fuels. The Paris Agreement of 2015 limits greenhouse gas (GHG) emissions to reduce global warming [1]. In this regard, many societies are transitioning to cleaner energy sources like wind and solar (renewables) to pave the way for deep electrification.

Context: Typically, distributed energy resources (DERs) are small, numerous, and dispersed throughout the distribution system. They are constantly being added, modified, and retired. Utility planning departments process connection requests for these DERs, performing power flow and hosting capacity studies. Such studies involve detailed engineering analyses, ensuring accurate DER representation based on the submitted connection applications.

Problem 1: The planning department receives and stores information for approving numerous small DER connections. However, this information is static and does not update over time to reflect reality, in contrast to the information and models required by utility operations. Bridging this gap is a herculean task that can appear insurmountable in deep electrification. This problem is further exacerbated when the actual power supply of connected DERs differs from their nameplate capacity due to capacity reduction, equipment fault, etc.

Problem 2: In the operations room of distribution utilities, deep electrification introduces countless small and scattered DERs throughout the system. It becomes significantly challenging for analytical tools such as the advanced distribution management system (ADMS) to capture all connected DER information, accurately represent connected DERs, and analyze or optimize the system effectively [2].

Problem 3: Finally, estimating the aggregate capacity and predicting the total power generation of the vast number of small and dispersed DERs connected across the system is challenging.

To address these challenges and facilitate the practical implementation of deep electrification, this paper emphasizes the estimation of the aggregate capacity of connected DERs, even when faced with limited information. Notably, this paper addresses the estimation of the aggregate capacity of connected DERs as a sequel to the hosting capacity problem. Following the resolution of the hosting capacity problem for a feeder, power system utilities need to understand the aggregate capacity of these connected DERs during the operational stage. This understanding aids in forecasting the total generation of these connected DERs and assessing their impact on the net load of the feeder, which will be addressed in this paper.

A. BACKGROUND AND LITERATURE REVIEW

The growing number of DERs are reshaping modern power systems. Integrating DERs extensively and managing the uncertainty involved in this integration is key to establishing a smart distributed energy system [3]. In general, a DER is ''any resource on the distribution system that produces electricity and is not otherwise included in the formal North American Electric Reliability Corporation (NERC) definition of the Bulk Electric System'' [4]. The rising integration of renewable energy and electric vehicles (EVs) in distribution grids introduce complexity and uncertainty, necessitating innovative solutions in grid management. DERs, while environmentally beneficial, can shift the system's net load profile by acting as a ''negative demand.'' This shift emphasizes the importance of accurate net load forecasting, especially with invisible solar and wind generation [5]. Therefore, power professionals face challenges in making short-term load forecasting (STLF) [6]. Since STLF focuses on near-future forecasting, time, date, and weather conditions are the most considered features to predict future load values [7]. Generally, the aggregated level's diversity smooths the daily load profile, resulting in a more predictable substation load.

Several forecasting methods have been applied for these time domains, including statistical models and artificial intelligence (AI) techniques [8], [9]. AI methods, specifically artificial neural networks (ANNs), have gained popularity over the past few decades. To predict energy demand, an ensemble deep learning-based method is proposed in [10],

and a hybrid deep learning model is described in [11]. Despite the benefits of forecasting techniques, challenges related to prediction accuracy still exist.

Convolutional long short-term memory (CNN-LSTM), a type of deep neural network (DNN), shows promise in addressing these challenges [12], [13]. This paper delves deeper into the potential of hybrid models, particularly the CNN–LSTM architecture, for enhancing the accuracy and reliability of DER aggregate forecasting.

B. INTEGRATION AND MANAGEMENT OF DERs IN ADMS

Advanced distribution management systems are increasingly utilized in the operation of modern large distribution systems [14], [15]. A review of the challenges for integrating emerging DERs into ADMS modeling is given in [16] and [17]. In the march toward deep electrification, two main elements, built on renewables and using ADMSs, are critical to the operations and control of distribution systems: 1) novel methods for estimating the capacity of DERs connected to a feeder; and 2) computationally efficient forecasting of feeder flows that connect innumerable DERs.

The lack of detailed information on individual connected DERs presents a significant obstacle to effectively modeling and optimizing distribution systems using ADMS [18]. The efficiency of an ADMS depends heavily on the completeness and accuracy of input data, including DER characteristics, capacities, and locations. Existing ADMS methods often rely on nameplate-based representations of DERs, which may lead to inaccuracies and suboptimal management of distribution networks [14].

To tackle these challenges, this paper proposes an aggregate representation of DERs connected to lateral feeders. This model, trained over time, prioritizes actual output power over nameplate capacities, offering a more accurate estimation of overall generation capacity and future power output. By focusing on output-based representations, utilities can improve forecasting accuracy and overcome limitations posed by incomplete information about connected DERs. This approach offers a solution to the current challenges faced by ADMS methods in optimizing distribution systems.

C. CHARACTERIZING THE AGGREGATE DER CAPACITY

DERs, often invisible to power system operators, play a pivotal role in deep electrification for system planning and operation. However, determining their aggregate capacity is not straightforward, given their diverse nature, fluctuating capacities, and widespread locations. Methods for power output forecasting from large-scale PV systems are described in [19] and [20]. Addressing data limitations, both [21] and [22] introduce probabilistic approaches to forecasting DER power. Additionally, methods for forecasting behind-the-meter (BTM) PV generation, relying on net-metered demand and local weather data, are discussed in [23] and [24]. The authors in [25] introduce a technique for simultaneous disaggregation of BTM solar and wind generation but struggle to accurately estimate aggregate capacity, highlighting a critical gap. Discussions on aggregated system-level solar power production, along with reliable forecasting of PV system output for grid operators are found in [26] and [27]. Consistently tracking installed capacities for PV systems and wind turbines is essential for managing modern energy challenges. While some utilities require registration of installations, others rely on GIS mapping, which remains contentious due to reliability concerns [28], [29]. ANN models proposed in [30] and [31] estimate the output power of individual DERs.

Despite progress in DERs power forecasting, there remains a significant gap in estimating their aggregate capacity and forecasting their aggregate power with limited data availability. Existing literature primarily focuses on models that require detailed information on individual connected DERs through a feeder, making them impractical for medium voltage (MV) feeder-level analysis. Moreover, most aggregate models are utilized to a single DER type, overlooking the diverse sources on an MV feeder.

To address these challenges, this paper introduces a novel model aimed at estimating the aggregate wind power capacity (AWPC) and aggregate solar power capacity (ASPC) installed on a feeder, with a focus on the feeder's head-end perspective where the meter for reading feeder power flow is available. Additionally, the paper develops forecasting methods for predicting both the aggregate output power of these renewable sources and the aggregate load power of the feeder at the meter point. These advancements facilitate precise analysis of numerous DERs and optimize MV feeder operations. By enhancing planning and distribution operations within the extensive distribution system, this approach provides valuable insights for effective management and optimization strategies.

D. MOTIVATIONS AND CONTRIBUTIONS

With deep electrification powered by renewables such as wind and solar on the near horizon, distribution utilities must prepare for this certain future. Unlike bulk power systems with large central generators, each MV distribution feeder will connect and be powered by hundreds or thousands of controllable and uncontrollable DERs. Their operations, dependent on their owners, are anticipated to be less regimented than centralized bulk power systems. In this challenging and uncertain operating environment, distribution utilities will be tasked with managing feeder operations in real-time, ensuring a reliable supply. Therefore, utilities require knowledge of connected renewables capacities. Given the dynamic nature of renewables, the sum of their nameplate ratings will not equal the aggregate capacity of renewables online. This makes the rapid estimation of renewables connected to an MV distribution feeder an essential operation room requirement. Therefore, a reliable forecast of renewable capacity and power flow becomes vital for effective feeder

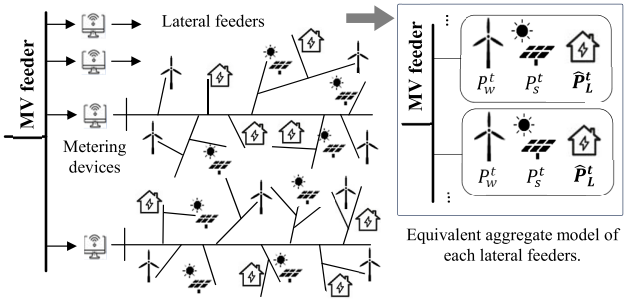

FIGURE 1. Schematic representation of aggregate models.

management. These considerations form the main motivations of this work.

Conducting a hosting capacity analysis is crucial for accurately assessing the quantity of DERs that can be safely integrated into the current power system structure [32]. This study extends beyond the hosting capacity analysis issue for a feeder, assuming that hosting capacity is already addressed and a substantial number of DERs are connected to the feeder. Consequently, utilities must ascertain the aggregate capacity of these connected DERs to assess their impact on system operation.

The primary objectives of this work are: 1) to estimate the aggregate capacities of renewables such as wind and solar connected to MV distribution feeders; and 2) to use these aggregate capacities of renewables (wind and solar) to derive high-resolution short-term forecasts.

The significant contributions of this work include:

1. A novel deep learning-based architecture for connected renewable generation and feeder flow representation, is detailed in Section II.
2. An innovative method for estimating the aggregate capacities of connected renewables to the lateral feeder, is described in Section II-B.
3. A high-resolution short-term training and forecasting algorithm, is presented in Section II-D.

The remainder of this paper is organized as follows. Section II introduces the proposed methodology and different DNNs used in the models. Section III discusses the result of each contribution, and Section IV concludes the paper.

II. THE PROPOSED METHODOLOGY

This paper aims to develop an aggregate equivalent model for an entire lateral of an MV feeder. This model is intended to accurately represent the aggregate performance of all connected DERs and loads for each lateral feeder, as shown in Fig. 1.

The methodology introduces a novel architecture comprising three distinct CNN-LSTM models tailored to wind, solar, and load power. The approach initially focuses on estimating the AWPC and ASPC installed on the lateral feeder.

With a comprehensive view of these connected DERs' overall capacity, power system operators can attain a deeper

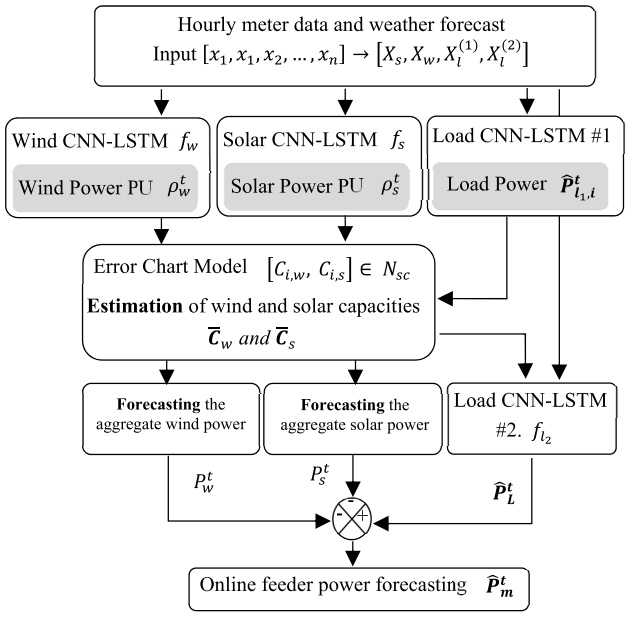

FIGURE 2. The architecture of the proposed model.

understanding of the entire system's generation capabilities. Following the capacity estimation, the approach then forecasts the hourly power generation for wind P_w^t and solar P_s^t, the aggregate load consumption along the feeder P_l^t, and the feeder power P_m^t. A detailed representation of the architecture is depicted in Fig. 2. This unique architecture stands as the primary contribution of this research, offering a more accurate and efficient method for estimating the aggregate capacity of the connected DERs and loads. This paper focuses on controllable DERs, specifically engineered to adjust their settings to maximize wind and solar generation power output. The control strategies of controllable DERs ensure maximum energy extraction by using available resources without storing them. The proposed methodology is divided into four parts, each of which will be elaborated upon in the subsequent subsections.

A. STEP 1: TRAINING OF WIND AND SOLAR PER UNIT (PU) MODELS

To formulate the aggregate output of the connected DERs, a CNN-LSTM model is utilized. For the wind model, the foundational dataset includes the date, time, wind speed, real-time weather data, and standard wind power p_w. Table 1 provides details of the weather datasets and inputs for the models used in this work. The weather data set is publicly available online at [33]. The resulting PU power ρ_w^t mirrors the hourly output profile expected from a wind turbine, as described in (1), where f_w represents the wind CNN-LSTM model.

In addition, a CNN-LSTM model, symbolized by f_s, is trained for solar power forecasting. It takes inputs like date, time, temperature, weather conditions, and solar power p_w,

TABLE 1. Overview of developed models and their inputs.

Model Name	Wind	Solar	Load	
			#1	#2
Input parameters	X_w	X_s	$X_l^{(1)}$	$X_l^{(2)}$
Date, time, and season	√	√	√	√
Temperature (°C)		√	√	√
Wind speed (m/s)	√			√
Precipitation, snowfall (mm/h)	√	√		√
Snow mass, radiation surface (kg/m^2)	√	√		√
Air density (kg/m^3), cloud cover	√	√		√
Radiation surface, and TOA (W/m^2)	√	√		√
Direct and diffuse irradiance (kW/m^2)		√		√
Target parameters	p_w	p_s	$P_{l,i}^t$	P_L^t

as detailed in Table 1. The output PU profile for solar is represented by ρ_s^t and outlined in (2). X_w and X_s show the input features for wind and solar models, respectively.

$$\rho_w^t = f_w(p_w, X_w) \tag{1}$$

$$\rho_s^t = f_s(p_s, X_s) \tag{2}$$

The target parameters for wind and solar CNN-LSTM models represent standard output power from these DER in PU, based on weather parameters. Given the lack of data on DERs, the total wind and solar power generated by each feeder remains unknown. Thus, this paper proposes using the pu profile of DER output as the target for training the wind and solar DNN models. These target parameters (denoted as p_w and p_s) are available in [33]. Each model is characterized by its own set of input features, with "√" indicating inclusion and " " indicating exclusion, as detailed in Table 1.

The input features for the DNN models encompass a range of environmental and temporal features essential for accurate energy forecasting, as detailed in Table 1. Date, time, and season provides temporal context, enabling the model to capture daily and seasonal energy demand fluctuations. Temperature and wind speed directly impact the performance of solar panels and wind turbines, respectively. Other parameters, such as snow mass, air density, cloud cover, and radiation surface, provide further details on environmental conditions influencing renewable energy generation. Direct and diffuse irradiance measurements reflect sunlight availability for solar power conversion, crucial for accurate solar energy predictions. By considering these diverse parameters, the DNN model can effectively capture the complex interactions between environmental factors and energy generation, enabling precise forecasting of DER performance and feeder load.

Existing literature in [8], [34], and [35] has already utilized CNN-LSTM for power prediction and demonstrated the effectiveness of this architecture in prediction tasks. Therefore, using this method for DER power prediction is not a contribution of this paper. The overall architecture of the CNN-LSTM model used in this paper is shown in Fig. 3.

Forecasting power at the feeder's head requires understanding the unique influences on load, solar, and wind power. Solar power depends on sunlight and temperature, while wind speed dynamics influence wind power. Even load forecasting has its specific factors. Using a separate DNN for each wind, solar, and load allows for greater accuracy tailored to their distinct characteristics. Using individual DNN models also improves predictions and enables an estimation of each DER's aggregate capacity separately. That is why three separate DNN models are used in this paper.

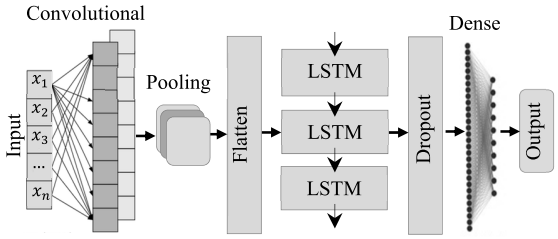

FIGURE 3. Architecture of the CNN-LSTM model for time-series predictions [8].

In assessing the broader regional impacts of meteorological conditions on energy generation, it is crucial to contextualize the inherent heterogeneity of both solar and wind resources. Individual solar panels and wind turbines might experience diverse conditions due to localized factors, leading to prediction deviations. By integrating the generation metrics from all DERs in the region, deviations balance out. At a larger scale, these discrepancies converge to an equilibrium, making the aggregate energy forecast more consistent. In [36], the smoothing effect is employed to mitigate the uncertainty associated with the total output of wind turbines. The proposed approach assumes a level of homogeneity in the solar and wind power profiles as they respond to the ambient environment.

B. STEP 2: DERs' CAPACITY ESTIMATION

One of the main challenges addressed in this paper is estimating the aggregate capacity of connected DERs in the absence of comprehensive technical details about the DERs and feeders. Considering that lateral feeders often contain numerous small DERs whose presence, state of repair, and actual performance deterioration over time may not be known to utilities and are scattered throughout the feeder. Thereby tracking them and predicting their output for making operational decisions becomes challenging. This lack of awareness regarding the actual functioning number and location of these DERs complicates power flow management. This section aims to address this challenge by estimating the aggregate capacity of each type of DER connected to the feeder, as observed from the meter at the feeder's head end. By aggregating the capacities of these DERs, distribution system operators can analyze their collective impact on feeder power flow and net demand without requiring specific information about individual DER installations. Therefore, it is assumed that the only technical data available is the feeder power flow reading from the meter located at the feeder's head end.

To address this challenge, an enumeration-based algorithm is proposed to estimate the AWPC and ASPC installed on the lateral feeder. This method considers multiple scenarios labeled as $i \in \{1, 2, \ldots, N_{SC}\}$. Within each scenario i, unique capacity values for aggregate wind and solar are allocated, represented as $C_{w,i}$ and $C_{s,i}$, respectively. The allocated capacities are considered from a minimum value and increase step by step until the maximum capacity is reached. Each step's capacity increase, known as the step size, along with the number of steps, are parameters that can be determined during the model development. To calculate the aggregate output power of wind and solar, the PU output, denoted as ρ and developed in Section II-A, is multiplied by the respective aggregate capacities of wind and solar considered for each scenario.

The aggregate output power of wind and solar in each scenario is represented by $P^t_{w,i}$ and $P^t_{s,i}$, and shown in (3) and (4).

$$P^t_{w,i} = \rho^t_w \times C_{w,i} \tag{3}$$

$$P^t_{s,i} = \rho^t_s \times C_{s,i} \tag{4}$$

For each scenario i, utilizing (5), the aggregate load power on the feeder, represented by $P^t_{l,i}$, is calculated for each time interval $t \in \{1, 2, \ldots, T\}$. This calculation is achieved by adding the feeder power (meter data) P^t_m to the aggregate power of the DERs.

$$P^t_{l,i} = P^t_m + \rho^t_w \times C_{w,i} + \rho^t_s \times C_{s,i} \tag{5}$$

Once the load power is computed for each scenario, the CNN-LSTM load model #1 for the i^{th} scenario, represented as $f^{(i)}_{l_1}$, is trained using (6).

$$\hat{\boldsymbol{P}}^{\boldsymbol{t}}_{\boldsymbol{l_1,i}} = f^{(i)}_{l_1}(P^t_{l,i}, X^1_l) \tag{6}$$

$\hat{\boldsymbol{P}}^{\boldsymbol{t}}_{\boldsymbol{l_1,i}}$ is the predicted load power derived from the load model #1 for each scenario. $P^t_{l,i}$ is the target value in the training process calculated in (5). X^1_l represents the input feature for this model #1, as detailed in Table 1, comprising only temperature and datetime. This choice is made because these features do not correlate with the outputs of the wind and solar models. This non-correlation ensures that the scenario providing the most accurate estimation of wind and solar aggregate capacities will yield the smallest error in the error chart.

Therefore, load model#1 is developed for each scenario, and its performance is evaluated using root mean square error (RMSE) as delineated in (7), where T represents the total number of timesteps. An error chart showcasing the $RMSE_i$ values across all scenarios is constructed after calculating the error for each. Using the error chart, the model identifies the scenario with the least RMSE. Wind and solar capacities corresponding to the scenario with the least $RMSE_i$ are chosen as the estimated AWPC and ASPC, represented by $\bar{\boldsymbol{C}}_w$ and $\bar{\boldsymbol{C}}_s$, respectively.

$$RMSE_i = \sqrt{\left(\frac{1}{T}\right) \times \sum_{j=1}^{T} \left(\hat{\boldsymbol{P}}^{\boldsymbol{t}}_{\boldsymbol{l_1,i}} - P^t_{l,i}\right)^2} \tag{7}$$

1) NARROWING SEARCH SPACE

Given that the wind and solar power values in each scenario are determined discretely, the difference in power between two consecutive scenarios can be defined as the "step size." Commencing from zero and progressing to the maximum capacity for both wind and solar encompasses a multitude of scenarios. Employing a larger step size risks affecting the model's accuracy because actual capacity could lie between two consecutive scenarios, while smaller steps can increase processing time. To address this, a method is introduced to reduce the training time while preserving model accuracy. This approach involves calculating load values for all scenarios based on (5). Subsequently, the load values across various scenarios undergo filtering to remove any scenarios resulting in load data containing negative values. This is essential as load power is always expected to be positive.

2) TRUST POINTS CONCEPT

Specific moments exist when both wind and solar output powers drop to near zero based on the meteorology situation. At these time steps, the calculated load power, which is the outputs of (5), across various scenarios converge, displaying minimal variation. These crucial time steps are termed Trust Points (TP) in this study. These points depict time steps when the load power in all scenarios confidently aligns with the actual load power it aims to predict. Training the model using these TPs ensures a more reliable prediction, as the TP load power closely mirrors the real-world load power. When trained using these TPs, the model exhibits minimal deviation, especially around the true wind and solar capacity values. However, the training dataset also incorporates non-TP instances for a holistic training experience. This mixed approach aids in refining the model's predictability, ensuring it can predict loads with the least RMSE. For the scope of this research, a TP is explicitly defined as a point where the wind and solar output powers, as per the PU output profile detailed in Section II-A, are below 0.15 and 0.05 PU, respectively. Testing has shown that these TP values yield optimal model performance.

C. STEP 3: MODEL DEVELOPMENT AND OFFLINE FORECASTING

Upon estimating the AWPC and ASPC based on the minimum value in the error chart, a refined load prediction model using a CNN-LSTM can be established. Utilizing (8), the actual load data, P^t_L, can be deduced since all the variables on the right-hand side of this equation have already been discerned from previous steps. P^t_m is the hourly feeder power data, which serves as an input for the model. ρ^t_w and ρ^t_s are the PU power profiles of wind and solar, trained in section II-A,

and $\bar{C}_w$ and $\bar{C}_s$ are the AWPC and ASPC, estimated in section II-B. Therefore, the aggregate load power for the feeder can be derived based on (8). This equation illustrates the interplay between the load to the feeder power, wind power, and solar power.

$$P_L^t = P_m^t + \rho_w^t \times \bar{C}_w + \rho_s^t \times \bar{C}_s \tag{8}$$

This calculated P_L^t data, combined with date, time, and weather, forms the input features for load model #2 (X_l^2). Here the load model uses all time-related and weather-related input features to make the most accurate prediction of future load and develops a model that can predict the aggregate load power for the feeder. Once these input features are prepared, load model #2 is trained. This model, represented as f_{l_2}, can forecast the load power for each feeder. The structure of the CNN-LSTM for load model #2 is the same as that of the first load model, with the difference being that here, all input features are used to create an accurate model for load forecasting. Following the successful training, future aggregate load data predictions ($\hat{\boldsymbol{P}}_{\boldsymbol{L}}^{\boldsymbol{t}}$) become attainable using (9).

$$\hat{\boldsymbol{P}}_{\boldsymbol{L}}^{\boldsymbol{t}} = f_{l_2}(P_L^t, X_l^2) \tag{9}$$

D. STEP 4: ONLINE OPERATIONAL STAGE

In this stage, the method enters an online mode to forecast future feeder power flow. Once the DNN models for wind, solar, and load are trained and available, and the aggregate capacities of the DERs for each feeder are estimated, the feeder power at head-end can be predicted in online operational mode, as shown in (10).

$$\hat{\boldsymbol{P}}_{\boldsymbol{m}}^{\boldsymbol{t}} = f_{l_2}(X_l^2) - \bar{C}_w \times f_w(X_w) - \bar{C}_s \times f_s(X_s) \tag{10}$$

In this equation, $\hat{\boldsymbol{P}}_{\boldsymbol{m}}^{\boldsymbol{t}}$ shows the predicted feeder power at time t. With the aggregate capacities for wind and solar already determined and the respective CNN-LSTM models for each feeder in place, forecasting the feeder data for each feeder requires only the forecasted weather dataset. It is important to note that wind, solar, and load power values are mentioned as target parameters in Table 1, so there is no need to include these parameters in the online stage.

The model operates on an hourly basis, allowing for detailed intra-day predictions of renewable energy generation and load consumption. This enables distribution system operators to make more informed decisions in real-time, optimizing system performance and resource allocation throughout the day. By leveraging hourly data inputs, the model can accurately forecast the aggregate output of DERs, total load demand, and feeder power for each time step.

Further, this can be applied to all feeders and the power system operators will have insight into the flow of power on the feeders for each hour, just by using the forecasted weather data. The proposed operational stage of the model which can work in an online mode, serves as the third innovation of this work. This predicted feeder power serves as invaluable information for decision-making processes within distribution system operations, enabling operators to anticipate and plan for fluctuations in energy demand, optimize resource allocation, and efficiently manage grid operations. Additionally, it provides crucial insights for network reconfiguration, allowing operators to make informed decisions regarding network adjustments, equipment maintenance, and system enhancements to ensure the reliability, and resilience of the distribution systems.

E. COMPLETE ALGORITHM

In the enumeration-based algorithm proposed in this paper, the challenge lies in the absence of detailed data regarding individual DERs connected to the feeder. Without specific information on the capacities of each DER, determining the aggregate power generation becomes challenging. Given that only feeder power data and a weather dataset are available, the aggregate power generation from DERs remains unknown for each feeder instance. Consequently, there are no target values available for training the DNN models for wind and solar power prediction.

To overcome data limitation, the decision is made to train the DNN models to predict the PU profile for the feeder. By setting the target value for wind and solar power as 1 PU (equivalent to 1 MW in this paper), the models are trained to discern the relative proportions of wind and solar power generation.

During the enumeration-based algorithm, different scenarios representing varying aggregate capacities for wind and solar generators are considered. By evaluating the error chart for the training of load CNN-LSTM model, the algorithm identifies the scenario (best capacities for wind and solar generation) that best aligns with the observed feeder power data and weather conditions. This process facilitates the estimation of the aggregate capacities of wind and solar generators connected to the feeder, despite the lack of detailed information on individual DER capacities.

Subsequently, with the estimated aggregate capacities of wind and solar generators, the trained PU profile enables the forecast of aggregate wind and solar generation. This forecasting capability is pivotal for anticipating the overall renewable energy contribution to the feeder's power flow.

The proposed methodology for aggregate capacity estimation and feeder power forecasting is described below. In addition, the accompanying flowchart in Fig. 4 summarizes the entire process and the steps the models take to estimate the aggregate capacity of connected DERs and forecast the feeder power.

The proposed model steps to estimate the aggregate capacity of the connected derS and forecast the feeder power include:

Step 1: Data collection and initial training.

- Gather weather and technical datasets.
- For each DER, develop and train the CNN-LSTM module (f_s and f_w) to forecast the PU output power (ρ_w^t and ρ_s^t).

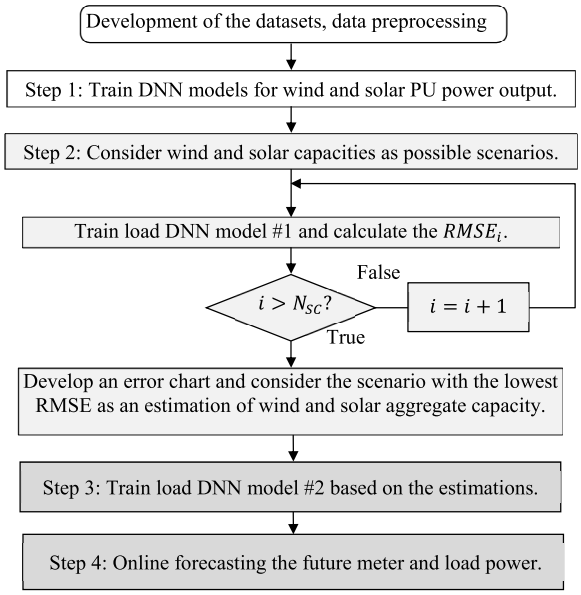

FIGURE 4. **Flowchart outlining the aggregate capacity estimation and power forecasting process.**

- Wind and solar models for a specific feeder are now trained and available.

Step 2: DER Capacity estimation.

- Use an enumeration-based approach to consider various wind and solar capacity combinations ($C_{w,i}$, $C_{s,i}$), denoted as potential scenarios $i \in \{1, 2, \ldots, N_{SC}\}$.
- For each scenario i, compute the corresponding load power $P^t_{l,i}$ using equation (5) and train load model #1 accordingly.
- Calculate the $RMSE_i$, comparing the $P^t_{l,i}$ and $\hat{\boldsymbol{P}}^{\boldsymbol{t}}_{\boldsymbol{l,i}}$.
- Repeat the process for each scenario to create an error chart highlighting $RMSE_i$ values for all scenarios.
- Determine the capacities $\bar{\boldsymbol{C}}_w$ and $\bar{\boldsymbol{C}}_s$ that correspond to the minimum $RMSE_i$ as the estimated capacities.
- Enhance the estimation accuracy by developing a new error chart by modifying the scenario ranges, increasing the N_{SC} or decreasing the power per step.

Step 3: Load power forecasting and offline training stage.

- Train the CNN-LSTM load model #2 using the estimated capacities and forecasted DER power values.
- The Load model #2 for a specific feeder is now trained and available.

Step 4: Online operation.

- The DNN models for wind, solar, and load for each feeder are already trained and available.
- The aggregate capacity for each feeder is estimated.
- The feeder power flow can be forecasted using (10).

III. RESULTS

In this section, the effectiveness of the proposed methodology is evaluated using hourly meter data obtained from an actual meter located at the top of a North American utility feeder.

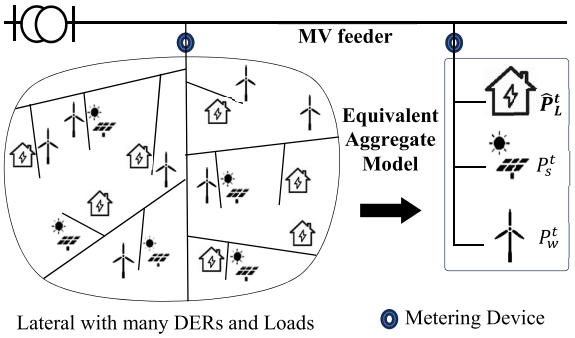

FIGURE 5. **The aggregate representation of the lateral feeder.**

A diverse range of scenarios has been considered in these experiments. Notably, the peak value recorded in the meter data reached approximately 20 MW without any DER installation. Weather data and actual standard DER power were obtained from a publicly available online source [33]. This dataset, adjustable for specific locations and times, served as the foundation for the analysis.

These results provide valuable insights into the performance and applicability of the proposed methodology in real-world utility feeder scenarios, demonstrating its effectiveness in accurately estimating aggregate capacities and forecasting feeder power under various conditions.

A. ALGORITHM PERFORMANCE

This work aims to develop an equivalent model representing an entire lateral feeder connected to an MV feeder, aggregating the performance of connected DERs and loads. Separate models are utilized to depict their respective performance. Figure 5 illustrates the aggregate representation of the entire lateral feeder, enabling system operators to make decisions based on the aggregate performance of DERs and loads rather than individual units.

The architecture of the DNN model is specifically formed for output power predictions, combining CNN and LSTM techniques for training, as illustrated in Fig. 3 [8]. Initially, a CNN layer is employed to learn spatial hierarchies from the data, followed by a pooling layer to reduce spatial dimensions.

A flattening layer is then utilized to reshape and flatten the data, ensuring compatibility with the subsequent LSTM layers. Then, LSTM layers are integrated to enable the model to capture recent patterns and understand long-term dependencies within the input data. The output from the first LSTM layer serves as input for the creation of the second LSTM layer. To mitigate overfitting, a dropout layer is incorporated, randomly deactivating some neurons during training. Finally, a dense layer provides the ultimate prediction.

During model training, 80% of the dataset is utilized for training, while the remaining 20% is reserved for testing to assess the model's accuracy. Notably, the predicted wind and solar power closely align with the actual power values,

TABLE 2. Configuration of DNN models.

Hyperparameters	Solar and wind Model	Load Model #1	Load Model #2
Input Features	X_s, X_w	$X_l^{(1)}$	$X_l^{(2)}$
CNN layers	1	1	2
Number of filters	16	16	32
Kernel size	[2×2]	[2×2]	[2×2]
Pooling type	Max	Max	Max
LSTM layers	2	2	3
Number of neurons	32/16	32/16	32/32/16
Activation function	ReLU	ReLU	ReLU
Loss function	MSE	MSE	MSE
Optimizer	Adam	Adam	Adam
Learning rate	0.001	0.001	0.001
Batch size	32	32	32
Epochs	50	50	100
Dropout	0.3	0.3	0.2
Training data split	80%	80%	80%
Performance metric	RMSE	RMSE	RMSE

showing an RMSE of 1.15% for solar predictions and 2.34% for wind predictions.

All models adopt the Rectified Linear Unit (ReLU) activation function due to its efficiency and effectiveness in various prediction tasks. The mean squared error (MSE) loss function is employed to quantify the disparity between predicted and actual values. Optimization is achieved through the Adam optimizer, for its computational and memory efficiency. A suitable learning rate is meticulously chosen to ensure steady convergence during training. Furthermore, the models are trained with a batch size carefully selected to set a balance between learning efficiency and gradient descent process stability.

The hyperparameters across different DNN models are meticulously tuned to optimize each model's performance. While the structural architecture remains consistent across models, specific hyperparameters such as the number and size of CNN and LSTM layers, the number of neurons, activation functions, etc., are varied. Table 2 provides a comprehensive overview of the configuration of the DNN models, encompassing various hyperparameters such as input features, number of layers, activation functions, epochs, loss functions, optimizers, learning rates, batch sizes, dropout rates, training data splits, and performance metrics. Each hyperparameter is tailored to suit the specific requirements of the model, ensuring optimal performance across different prediction tasks.

B. TEST CASES

The initial meter data does not include any wind and solar penetration. To assess the efficacy of the proposed model, meter data was adjusted by subtracting five different wind and solar values. This revised meter data, which represents varying levels of DER penetration, was then used as five distinct test cases. Each test case features a unique wind-to-solar power penetration ratio, as indicated by Roman numerals in Table 3. For estimating the aggregate capacity and forecast power for each test case, various scenarios were examined, each characterized by distinct wind and solar capacities ($C_{w,i}$ and $C_{s,i}$). The considered scenarios for each test case are shown by N_1 to N_{36} in Table 3. All 36 scenarios - enumerated in Table 3 - are considered for all five test cases to maintain consistency throughout the paper.

TABLE 3. Wind and solar capacities in different scenarios.

Test cases (I-V) Scenarios (N_1-N_{36})		$C_{w,i}$ (MW)					
		3	**6**	**9**	**12**	**15**	**18**
$C_{s,i}$ (MW)	**3**	N_1	N_2	N_3	N_4	N_5	N_6
	6	N_7	N_8	***III***	***IV***	***V***	N_{12}
	9	N_{13}	N_{14}	N_{15}	N_{16}	N_{17}	N_{18}
	12	N_{19}	***I***	N_{21}	***II***	N_{23}	N_{24}
	15	N_{25}	N_{26}	N_{27}	N_{28}	N_{29}	N_{30}
	18	N_{31}	N_{32}	N_{33}	N_{34}	N_{35}	N_{36}

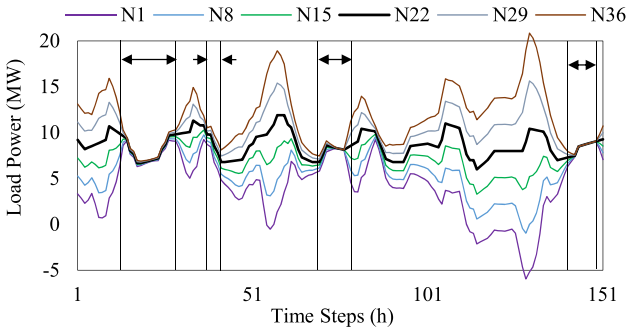

FIGURE 6. Load power $P_{l,i}^t$ for different scenarios N in test case II.

For instance, the first test case exhibits a wind power to solar power penetration ratio of 0.5, implying that the aggregate capacity of wind connected to the feeder is 6 MW and the aggregate capacity of solar connected to the feeder is 12 MW. The subsequent test cases have 1, 1.5, 2, and 2.5 wind-to-solar ratios. The model's goal is to, for each test case, accurately estimate the actual aggregate capacities of connected wind and solar ($\bar{C}_w$ and $\bar{C}_s$) among the considered scenarios.

In Table 3, the capacities of the scenarios range from 3 MW to 18 MW, with the step size set to 3 MW for both wind and solar. The load power corresponding to all these scenarios is calculated using (5). Since load power cannot be negative, any scenario resulting in a negative load power value is excluded from the available scenarios to expedite computations. Fig. 6 illustrates the load power across various scenarios for test case II, in which scenario N_{22} shows the actual load power for this test case. In this figure, arrows highlight the TP moments, during which the load power in all scenarios closely aligns with the actual load power.

Upon evaluating all scenarios for each test case, an error chart can be generated. Figure 7 shows the error chart for test case II, where the model computes $RMSE_i$ values for all scenarios based on the actual and predicted load using load

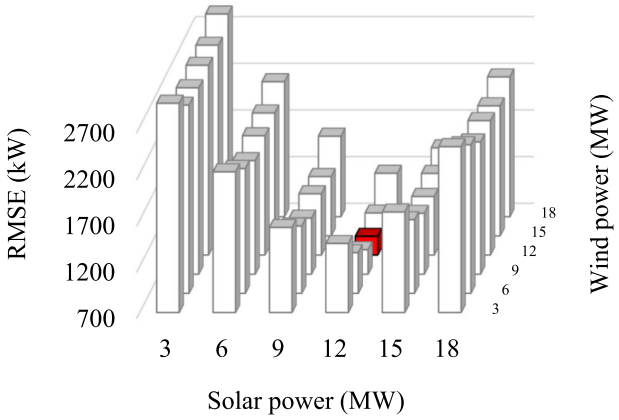

FIGURE 7. **Error chart for test case II, AWPC = ASPC = 12 MW.**

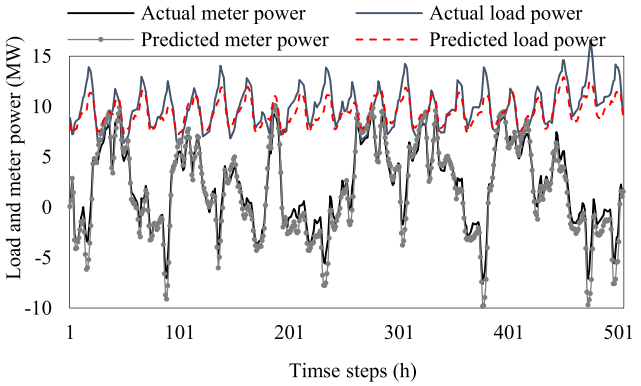

FIGURE 8. **Actual and forecasted load power and feeder power (MW) in test case II.**

TABLE 4. **Accuracy metric for all test cases, step size = 3MW.**

Test case	$\bar{C}_s$	$\bar{C}_w$	Accuracy load %	Accuracy feeder %	Correct Estimation
I	12	6	95.78	93.71	Yes
II	12	12	95.86	93.91	Yes
III	6	9	95.47	93.56	Yes
IV	6	12	95.68	93.98	Yes
V	6	15	95.67	93.46	Yes

model #1. In this error chart, the model effectively estimates the correct aggregate capacity of connected wind and solar ($\bar{C}_w$ and $\bar{C}_s$) to the feeder, highlighted in red. Hence, an error chart is generated for each test case based on the available scenarios. The scenario with the lowest RMSE error value in the error chart is then selected as the estimated capacity of connected DERs. This result corresponds to contribution #2, outlined in Section II-B.

The results presented in Table 4 provide a comprehensive evaluation of the model's performance across all the test cases. The table provides detailed information on the RMSE and the accuracy of the model's forecasting ability for future load and meter power across all test cases. Additionally, the estimated capacities in each test case, denoted as $\bar{C}_w$ and $\bar{C}_s$, are presented in the table. The proposed method accurately estimates the AWPC and ASPC installed, among all the available scenarios for each test case.

The 'Accuracy' metric, calculated by deducting the RMSE percentage from 100%, provides a measure of how closely the model's forecasted meter power aligns with the actual power observed in the feeders. It offers quantifiable insight into the precision of the model's predictions, confirming its suitability for practical application.

Table 4 shows that the model achieves an average accuracy rate of 95.69% for load power forecasting and 93.72% for feeder power forecasting across all test cases while using a step size of 3 MW. This high level of precision underscores the model's ability to accurately forecast future power flowing at the head of the feeder, even when numerous unknown DERs are connected to the feeder. The consistent performance metric demonstrates the reliability of the model's predictions.

The 'Correct Estimation' column in Table 4 confirms the reliability of the model, indicating accurate estimation across all scenarios. For all test cases I to V, the proposed method was able to estimate the correct aggregate capacity of connected DERs among the considered scenarios. This column serves as a testament to the model's robustness and its potential applicability in real-world settings.

After estimating the $\bar{C}_w$ and $\bar{C}_s$, and having the trained wind and solar DNN models available, load model #2 can be trained based on (9). This training process enables the forecast of the aggregate load power for a lateral feeder, as illustrated in Figure 8. The RMSE error for the aggregate load power forecasting for test case II, shown in this figure, is 4.14%. This error value provides insight into the accuracy of the load forecasting model, with lower values indicating better predictive performance.

Now, armed with all the necessary information for a feeder, including the estimated wind and solar capacities and the trained load forecasting model, feeder power can be forecasted during the online operational stage using (10). Figure 8 illustrates the comparison between the actual and predicted feeder power profiles for test case II. The error value is calculated at 6.09% for this test case, indicating the model's performance in forecasting feeder power. This result corresponds to contribution #3, as presented in Section II-D, and demonstrates the practical application of the proposed methodology in forecasting power consumption at the feeder level during real-time operations.

The analysis process for each test case is repeated five times, and the average error from these iterations for aggregate load forecasting is graphically represented in Fig. 9. This illustration reveals a relatively stable error percentage, hovering around 4.5%. This stability underscores the consistency and reliability of the proposed model in both estimating the aggregate capacity of connected DERs and forecasting feeder and load power at the MV feeder level.

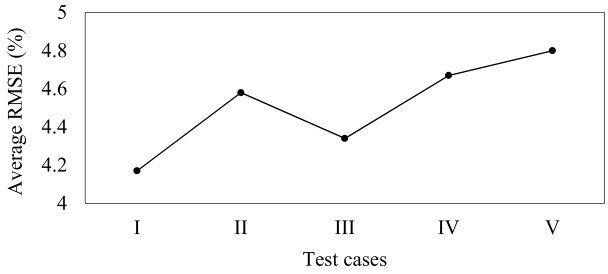

FIGURE 9. Average RMSE for different test cases.

TABLE 5. Estimated capacities and feeder power forecasting accuracy for different test cases and step sizes.

Test Case	Step size (MW)	$\overline{C}_w$ (MW)	$\overline{C}_s$ (MW)	Accuracy load power (%)	Accuracy feeder power (%)	Number of scenarios
	2	6	12	95.38	93.68	25
I	1	5	12	95.15	93.06	25
AWPC = 6 MW	0.5	6	12	95.45	93.62	49
ASPC = 12 MW	0.2	6	12.4	95.21	93.41	121
	0.1	6.2	11.9	95.32	93.51	121
	2	12	12	95.71	93.83	25
II	1	12	13	95.14	93.47	25
AWPC = 12 MW	0.5	12	11	95.04	92.96	49
ASPC = 12 MW	0.2	12.2	11.6	95.49	93.33	121
	0.1	12	12.2	95.30	93.27	121
	2	9	6	95.54	93.66	25
III	1	9	7	95.27	93.07	25
AWPC = 9 MW	0.5	8.5	6.5	95.33	93.19	49
ASPC = 6 MW	0.2	9	5.8	95.41	92.88	121
	0.1	9.1	6.1	95.58	93.58	121
	2	12	6	95.90	93.51	25
IV	1	12	6	95.66	93.48	25
AWPC = 12 MW	0.5	12	6.5	95.55	93.25	49
ASPC = 6 MW	0.2	11.8	6.4	95.38	92.93	121
	0.1	12.1	6.3	95.71	93.68	121
	2	15	6	96.00	93.62	25
V	1	15	7	95.25	93.06	25
AWPC = 15 MW	0.5	15.5	6.5	95.94	93.49	49
ASPC = 6 MW	0.2	15.2	5.6	95.03	92.82	121
	0.1	15.2	5.7	95.71	93.90	121

C. ANALYSIS FOR DIFFERENT STEP SIZES

In the previous section, the model utilized a step size of 3 MW, representing the difference between the capacities of two consecutive scenarios. However, it's possible that the actual AWPC and ASPC installed on the lateral feeder fall within the range considered for two consecutive scenarios.

To further explore this aspect, in this section, instead of having a 3 MW step size, the model is run using smaller step sizes of 2, 1, 0.5, 0.2, and 0.1 MW and evaluate capacity estimation algorithm, shown in Table 5. This table provides a comprehensive comparison of actual and estimated capacities, along with the errors in forecasted load and feeder power, for different step sizes. It enables an assessment of the model's performance under varying step sizes. Notably, the results demonstrate that the estimations of AWPC and ASPC closely align with the actual connected capacities, highlighting the model's accuracy in aggregate connected capacity estimation.

Initially, the scenarios are defined using a step size of 2 MW, resulting in 25 scenarios ($N_{SC} = 25$) plotted in the error chart. Specifically, in test case II, wind and solar capacities start at 8 MW, increasing by 2 MW per step, up to a maximum of 16 MW. This setup yields five capacity values for each wind and solar. Then the step size is reduced to 1 MW, for test case II, wind and solar capacities begin at 10 MW and increase by 1 MW per step until reaching 14 MW. This setup results in five capacity values for each and 25 scenarios ($N_{SC} = 25$) for the error chart. A smaller step size of 0.5 MW is adopted, leading to 49 scenarios ($N_{SC} = 49$). In test case II, wind and solar capacities start at 10.5 MW, progressing by 0.5 MW per step, and reach a maximum of 13.5 MW. This setup generates nine different capacity values for each wind and solar power.

Furthermore, a step size of 0.2 MW is employed, resulting in 121 scenarios ($N_{SC} = 121$). For instance, in test case II, wind and solar scenarios commence at 11 MW, increasing by 0.2 MW per step, and conclude at 13 MW. Finally, the smallest step size of 0.1 MW is utilized for further refinement, also leading to 121 scenarios ($N_{SC} = 121$). In test case II, wind and solar capacities start at 11.5 MW, incrementing by 0.1 MW per step, reaching a maximum of 12.5 MW, generating 11 different capacity values for each wind and solar power.

According to Table 5, the average accuracy in forecasting aggregate load and feeder power is 95.47% and 93.69%, respectively. These averages are calculated across all test cases and step sizes listed in the table.

The average error for estimating the aggregate capacities of wind and solar is also calculated based on the estimated capacities in Tables 4 and 5. To calculate the error in capacity estimation, the estimated capacity is subtracted from the actual capacity, and then divided by the actual capacity. Based on this calculation, the average error in estimating the aggregate capacity of DERs across all test cases and step sizes is 97.53%.

Running the models with larger step sizes may assist in approximating the range within which the AWPC and ASPC would fall. This approach saves time by avoiding the need to run the model for numerous scenarios. Once the model is run with a larger step size and an approximate range for the actual aggregate capacity is determined, the model can then be rerun using smaller step sizes near the estimated values from the previous run. This iterative process allows for a more refined estimation of the aggregate capacities while optimizing computational resources. On the other hand, if the precision and accuracy of the model in the first run are satisfying, there is no need for rerunning the model with smaller step sizes.

In Table 5, the number of scenarios corresponding to each step size is presented. An increase in scenarios leads to longer computational times for forecasting, yet the estimated capacity of DERs tends to align more closely with their actual installed capacity. Results indicate that varying the step size during model development does not significantly impact the

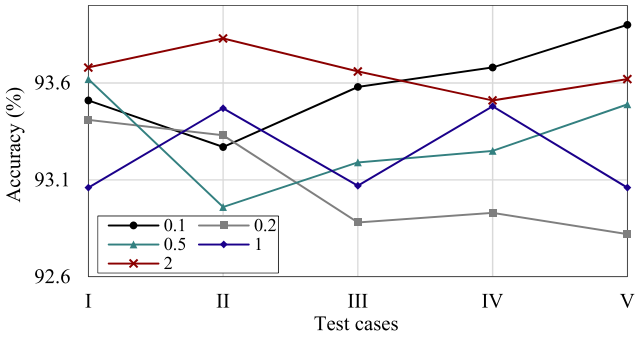

FIGURE 10. **Comparison of the feeder power flow forecasting accuracy for different step sizes over various test cases.**

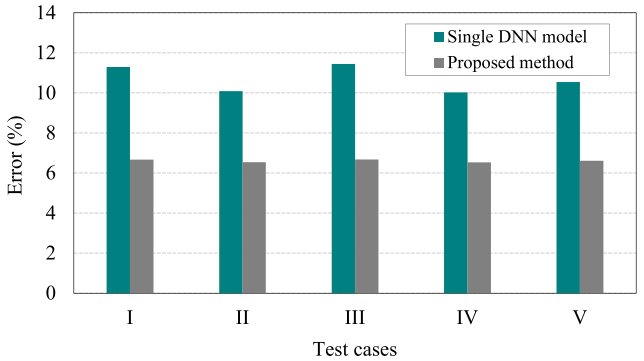

FIGURE 11. **Error comparison between the proposed method and a single DNN model for feeder power forecasting in each test case.**

accuracy of aggregated load and feeder power flow forecasts. Even when estimated capacities do not precisely match actual capacities, forecasting accuracy remains comparably high. This demonstrates the model's resilience in predicting future feeder power and load with reasonable precision. Figure 10 illustrates the feeder power flow forecasting accuracy across all test cases for varying step sizes, underscoring the model's stable performance despite changes in step sizes.

D. COMPARATIVE ANALYSIS WITH SINGLE DNN MODEL FOR FEEDER POWER FORECASTING

This section compares the proposed method with a single composite DNN model. The proposed method disaggregates wind, solar, and load powers, estimating the aggregate capacities of solar and wind generation. It trains separate models for solar, wind, and load power, each considering distinct input data sets, which enables the creation of specific and more accurate individual and collective forecasts. The model correlates solar power with irradiance and wind power with wind speed, while correlating load power with time and temperature. Load models are different for weekdays and weekends, whereas DER models are the same for all days. This external knowledge is bestowed upon the proposed model and is absent from single DNN models. Specifically, the single DNN model is not provided with the knowledge that solar power is highly correlated to irradiance and not with time, or that solar power is uncorrelated with the day of the week, whereas load is.

These are differences in the two models that manifest themselves in the forecast as illustrated in the following example. Consider an abnormal day with cloudy conditions in the afternoon such that solar irradiance is much lower than expected. In these circumstances, a single DNN model might produce an erroneous forecast correlating solar output to time, while the proposed method will produce a much more accurate forecast by correlating solar power exclusively to irradiance [5]. The reason for this inferior performance is that when the data set has abnormal input data points, a single DNN will train to minimize errors considering abnormal data points. However, the proposed method can distinguish these abnormal input data points and create better forecasts.

In contrast, a single DNN model creates a composite representation of feeder power flow comprising wind, solar, and load powers, training on weather and chronology data. Therefore, the separation of the feeder power into its components namely solar, wind, and load is not possible. The proposed method overcomes this challenge by initially estimating the AWPC and ASPC, and then developing a DNN model for aggregate load and feeder power prediction.

To demonstrate this aspect of the proposed method and assess the model's performance comprehensively, a single DNN model is trained using historical feeder power meter data as output, and weather and chronology datasets as inputs to directly forecast future feeder power. The architecture of this single DNN model corresponds to load model #2 as detailed in Table 2. The results of feeder power forecasting from the single DNN model are then compared with those from the proposed method. Figure 11 illustrates this comparison, demonstrating that the error value in forecasting the feeder power is lower in all test cases when using the proposed model. The results obtained for the proposed model are based on the average error in feeder power forecasting across all the step sizes. The overall average error for feeder power forecasting using the proposed method is 93.70%, while using a direct DNN model to predict the feeder power will lead to an average error of 89.32%.

Estimating the aggregate capacity of DERs while also predicting both feeder power and the total demand presents a complex challenge, particularly when only limited data from meter readings and weather forecasts are available. This research takes an innovative approach to these issues, contributing a distinct perspective not widely represented in existing literature. With the lack of directly established benchmarks for comparison, this study introduces a set of test cases tailored to evaluate the proposed approach. The results affirm the method's capability to produce accurate and effective estimates and forecasts.

E. DISCUSSION AND LIMITATIONS

This paper proposes a method for estimating connected aggregate capacities of renewable and load power, and thereafter uses this information for forecasting feeder power. The

DERs considered in the paper are wind and solar power generations. The proposed method can be extended to other types of renewables, with and without storage, which are controllable and otherwise. Differences in the operation of controlled and uncontrolled DERs will influence the performance of the proposed method and should be explored further. These may be undertaken by creating further CNN-LSTM modules in addition to solar and wind.

While denoting this as a shortcoming, future research will explore the inclusion of additional types of DERs into the model.

IV. CONCLUSION

This paper introduces a novel deep learning-based architecture aimed at addressing the challenge of estimating the aggregate capacity of connected DERs within a power system network, particularly when detailed information about individual DERs is unavailable. The primary goal is to equip distribution system operators with insights into the total power production from connected DERs and to provide accurate predictions of future power flow at the feeders.

Accurate estimation of aggregate DER capacity holds significant importance for informed decision-making in system reconfiguration, load balancing, and overall system control, particularly in distribution systems experiencing deep electrification and having numerous connected DERs. Unlike conventional approaches reliant on nameplate capacity, the proposed model adopts an output-based methodology, which proves more suitable in scenarios where detailed DER information is lacking or impractical to obtain.

The experimental results demonstrate the effectiveness of the model, with an average accuracy of 95.56% for forecasting aggregate load power, 93.70% for predicting future feeder power flow, and 97.53% for estimating the aggregate capacity of DERs. Moreover, the computational efficiency of the proposed model is noteworthy. For a North American distribution system comprising approximately 400 feeders and serving 1.4 million customers, our model can be individually trained for each feeder, on average, in less than 10 minutes. During the prediction phase, data processing per feeder occurs within seconds, facilitating real-time decision-making by distribution system operators.

Furthermore, the model's potential can be extended by incorporating other types of controllable and uncontrollable DERs, allowing for a more comprehensive representation of the system. These potential enhancements will be explored in future works.

REFERENCES

[1] United Nations Framework Convention on Climate Change (UNFCCC). *Process and Meetings: The Paris Agreement*. Accessed: Nov. 23, 2023. [Online]. Available: https://unfccc.int/process-and-meetings/the-paris-agreement

[2] US Department of Energy: National Renewable Energy Laboratory. *Grid Modernization: Advanced Distribution Management Systems*. Accessed: Nov. 23, 2023. [Online]. Available: https://www.nrel.gov/grid/advanced-distribution-management.html

[3] T. Morstyn, A. Teytelboym, and M. D. Mcculloch, "Bilateral contract networks for peer-to-peer energy trading," *IEEE Trans. Smart Grid*, vol. 10, no. 2, pp. 2026–2035, Mar. 2019.

[4] (Feb. 2017). *NERC Distributed Energy Resources—Connection Modeling and Reliability Considerations*. Accessed: Nov. 23, 2023. [Online]. Available: http://www.nerc.com/comm/Other/essntlrlbltysrvcstskfrcDL/Distributed_Energy_Resources_Report.pdf

[5] H. Shaker, H. Zareipour, and D. Wood, "A data-driven approach for estimating the power generation of invisible solar sites," *IEEE Trans. Smart Grid*, vol. 7, no. 5, pp. 2466–2476, Sep. 2016.

[6] W. Kong, Z. Y. Dong, Y. Jia, D. J. Hill, Y. Xu, and Y. Zhang, "Short-term residential load forecasting based on LSTM recurrent neural network," *IEEE Trans. Smart Grid*, vol. 10, no. 1, pp. 841–851, Jan. 2019.

[7] A. Azeem, I. Ismail, S. M. Jameel, and V. R. Harindran, "Electrical load forecasting models for different generation modalities: A review," *IEEE Access*, vol. 9, pp. 142239–142263, 2021.

[8] M. Alhussein, K. Aurangzeb, and S. I. Haider, "Hybrid CNN-LSTM model for short-term individual household load forecasting," *IEEE Access*, vol. 8, pp. 180544–180557, 2020.

[9] J. Wang, K. Wang, Z. Li, H. Lu, H. Jiang, and Q. Xing, "A multitask integrated deep-learning probabilistic prediction for load forecasting," *IEEE Trans. Power Syst.*, vol. 39, no. 1, pp. 1240–1250, Jan. 2024.

[10] J. Qin et al., "Multi-task short-term reactive and active load forecasting method based on attention-LSTM model," *Int. J. Electr. Power Energy Syst.*, vol. 135, Feb. 2022, Art. no. 107517.

[11] N. Jin et al., "Highly accurate energy consumption forecasting model based on parallel LSTM neural networks," *Adv. Eng. Informat.*, vol. 51, Jan. 2022, Art. no. 101442.

[12] F. A. Gers, J. Schmidhuber, and F. Cummins, "Learning to forget: Continual prediction with LSTM," *Neural Comput.*, vol. 12, no. 10, pp. 2451–2471, Oct. 2000.

[13] T. Y. Kim and S. B. Cho, "Predicting residential energy consumption using CNN-LSTM neural networks," *Energy*, vol. 182, pp. 72–81, Sep. 2019.

[14] Y. Fujimoto et al., "Distributed energy management for comprehensive utilization of residential photovoltaic outputs," *IEEE Trans. Smart Grid*, vol. 9, no. 2, pp. 1216–1227, Mar. 2018.

[15] W. Wu et al., "Integrated distribution management system: Architecture, functions, and application in China," *J. Modern Power Syst. Clean Energy*, vol. 10, no. 2, pp. 245–258, Mar. 2022.

[16] L. V. Strezoski et al., "Modeling challenges and potential solutions for integration of emerging DERs in DMS applications: Power flow and short-circuit analysis," *J. Modern Power Syst. Clean Energy*, vol. 7, no. 6, pp. 1365–1384, Nov. 2019.

[17] F. Pilo, G. Pisano, and G. G. Soma, "Advanced DMS to manage active distribution networks," in *Proc. IEEE Bucharest PowerTech*, Romania, Jun. 2009, pp. 1–8.

[18] *Advanced Dirstribution Management System*. Accessed: Nov. 23, 2023. [Online]. Available: https://www.se.com/ww/en/work/solutions/for-business/electric-utilities/advanced-distribution-management-system-adms/

[19] E. Nuño, M. Koivisto, N. A. Cutululis, and P. Sørensen, "On the simulation of aggregated solar PV forecast errors," *IEEE Trans. Sustain. Energy*, vol. 9, no. 4, pp. 1889–1898, Oct. 2018.

[20] S. Almaghrabi, M. Rana, M. Hamilton, and M. S. Rahaman, "Spatially aggregated photovoltaic power prediction using wavelet and convolutional neural networks," in *Proc. Int. Joint Conf. Neural Netw. (IJCNN)*, Shenzhen, China, Jul. 2021, pp. 1–8.

[21] J. Henze, M. Siefert, S. Bremicker-Trübelhorn, N. Asanalieva, and B. Sick, "Probabilistic upscaling and aggregation of wind power forecasts," *Energy, Sustainability Soc.*, vol. 10, no. 1, Mar. 2020.

[22] S. Camal, F. Teng, A. Michiorri, G. Kariniotakis, and L. Badesa, "Scenario generation of aggregated wind, photovoltaics and small hydro production for power systems applications," *Appl. Energy*, vol. 242, pp. 1396–1406, May 2019.

[23] N. Mahdavi, D. Weeraddana, and Y. Guo, "Probabilistic estimation of PV generation at customer and distribution feeder levels using net-demand data," *IEEE Trans. Smart Grid*, vol. 14, no. 3, pp. 1974–1984, May 2023.

[24] F. Bu, K. Dehghanpour, Y. Yuan, Z. Wang, and Y. Zhang, "A data-driven game-theoretic approach for behind-the-meter PV generation disaggregation," *IEEE Trans. Power Syst.*, vol. 35, no. 4, pp. 3133–3144, Jul. 2020.

[25] X. Liu et al., "Simultaneous estimation of behind-the-meter solar and wind power at the bulk supply point," *IEEE Access*, vol. 10, pp. 79703–79712, 2022.

[26] Y. Zhang, M. Beaudin, H. Zareipour, and D. Wood, "Forecasting solar photovoltaic power production at the aggregated system level," in *Proc. North Amer. Power Symp. (NAPS)*, Pullman, WA, USA, Sep. 2014, pp. 1–6.
[27] M. Rana, A. Rahman, and J. Jin, "A data-driven approach for forecasting state level aggregated solar photovoltaic power production," in *Proc. Int. Joint Conf. Neural Netw. (IJCNN)*, Glasgow, U.K., Jul. 2020, pp. 1–8.
[28] L. Waswa, M. J. Chihota, and B. Bekker, "A probabilistic estimation of PV capacity in distribution networks from aggregated net-load data," *IEEE Access*, vol. 9, pp. 140358–140371, 2021.
[29] J. Wang, W. Zheng, and Z. Li, "Detection and estimation of behind-the-meter photovoltaic generation based on smart meter data analytics," *Electr. J.*, vol. 35, no. 5, Jun. 2022, Art. no. 107132.
[30] C. Opathella, B. N. Singh, D. Cheng, and B. Venkatesh, "Intelligent wind generator models for power flow studies in PSS®E and PSS®SINCAL," *IEEE Trans. Power Syst.*, vol. 28, no. 2, pp. 1149–1159, May 2013.
[31] T. Xu, B. Venkatesh, C. Opathella, and B. N. Singh, "Artificial neural network model of photovoltaic generator for power flow analysis in PSS ® SINCAL," *IET Gener., Transmiss. Distribution*, vol. 8, no. 7, pp. 1346–1353, Jul. 2014.
[32] K. Lee, P. Zhao, A. Bhattacharya, B. K. Mallick, and L. Xie, "An active learning-based approach for hosting capacity analysis in distribution systems," *IEEE Trans. Smart Grid*, vol. 15, no. 1, pp. 617–626, Jan. 2024.
[33] S. Pfenninger and I. Staffell, "Long-term patterns of European PV output using 30 years of validated hourly reanalysis and satellite data," *Energy*, vol. 114, pp. 1251–1265, 2016.
[34] S. Hochreiter and J. Schmidhuber, "Long short-term memory," *Neural Comput.*, vol. 9, no. 8, pp. 1735–1780, Nov. 1997.
[35] C. Tian, J. Ma, C. Zhang, and P. Zhan, "A deep neural network model for short-term load forecast based on long short-term memory network and convolutional neural network," *Energies*, vol. 11, no. 12, p. 3493, Dec. 2018.
[36] C. Opathella and B. Venkatesh, "Managing uncertainty of wind energy with wind generators cooperative," *IEEE Trans. Power Syst.*, vol. 28, no. 3, pp. 2918–2928, Aug. 2013.

AMIR REZA NIKZAD received the B.Sc. and M.Sc. degrees in electrical engineering majoring in power systems from the University of Tehran, Tehran, Iran, in 2016 and 2019, respectively. He is currently pursuing the Ph.D. degree with the Centre for Urban Energy, Toronto Metropolitan University, Toronto, ON, Canada. His research interests include renewable energy resources and the application of machine learning in power systems.

AMR ADEL MOHAMED (Senior Member, IEEE) received the Ph.D. degree from Toronto Metropolitan University (formerly Ryerson), Toronto, ON, Canada, in 2019. He is currently an Assistant Professor with Cairo University, Cairo, Egypt, and an Adjunct Professor with Toronto Metropolitan University. His research interests include power system optimization, energy storage, and renewable energy resources. He is a Registered Professional Engineer in the province of Ontario, Canada.

BALA VENKATESH (Senior Member, IEEE) received the Ph.D. degree from Anna University, Chennai, India, in 2000. He is currently a Professor and the Academic Director of the Centre for Urban Energy, Toronto Metropolitan University, Toronto, ON, Canada. His research interests include power system analysis and optimization. He is a Registered Professional Engineer in the province of Ontario, Canada.

JOHN PENARANDA received the B.Sc. degree in electrical engineering from Universidad Mayor de San Simon, Bolivia, in 1991, the M.Sc. degree in renewable energies from Universidad Internacional de Andalucía, Spain, 1997, and the M.B.A. degree from Southern Adventist University, Collegedale, TN, USA, in 2002. In 2009, he joined Hydro One, where he is currently the Grid Operations Manager of the Operating Engineering-Project Enablement Group. He has more than 25 years of experience in power systems engineering applied to transmission and distribution grids. He is a Professional Engineer with Professional Engineers Ontario (PEO) and a Fellow Engineer Canada (FEC). He is also the past-Chair of the Willowdale/Thornhill Chapter of PEO.